The Astrophysical Journal Letters, 723:L134–L138, 2010 November 10 doi:10.1088/2041-8205/723/2/L134

DETECTION OF LARGE ACOUSTIC ENERGY FLUX IN THE SOLAR ATMOSPHERE

N. Bello González[1], M. Franz[1], V. Martínez Pillet[3], J. A. Bonet[3], S. K. Solanki[2,7], J. C. del Toro Iniesta[4], W. Schmidt[1], A. Gandorfer[2], V. Domingo[4], P. Barthol[2], T. Berkefeld[1], and M. Knölker[6]
[1] Kiepenheuer-Institut für Sonnenphysik, Schöneckstr. 6, 79110 Freiburg, Germany; nbello@kis.uni-freiburg.de
[2] Max-Planck-Institut für Sonnensystemforschung, Max-Planck-Strasse 2, 37191 Katlenburg-Lindau, Germany
[3] Instituto de Astrofísica de Canarias, Avd. Vía Láctea s/n, La Laguna, Spain
[4] Instituto de Astrofísica de Andalucía (CSIC), Apdo. de Correos 3004, 18080 Granada, Spain
[5] Grupo de Astronomía y Ciencias del Espacio, Universidad de Valencia, 46980 Paterna, Spain
[6] High Altitude Observatory, National Center for Atmospheric Research, Boulder, CO 80307, USA
[7] School of Space Research, Kyung Hee University, Yongin, Gyeonggi, 446-701, Republic of Korea
Received 2010 June 16; accepted 2010 September 16; published 2010 October 15

ABSTRACT

We study the energy flux carried by acoustic waves excited by convective motions at sub-photospheric levels. The analysis of high-resolution spectropolarimetric data taken with IMaX/Sunrise provides a total energy flux of ∼6400–7700 W m^{-2} at a height of ∼250 km in the 5.2–10 mHz range, i.e., at least twice the largest energy flux found in previous works. Our estimate lies within a factor of two of the energy flux needed to balance radiative losses from the chromosphere according to the estimates of Anderson & Athay and revives interest in acoustic waves for transporting energy to the chromosphere. The acoustic flux is mainly found in the intergranular lanes but also in small rapidly evolving granules and at the bright borders, forming dark dots and lanes of splitting granules.

Key words: Sun: chromosphere – Sun: oscillations – Sun: photosphere – techniques: high angular resolution – techniques: spectroscopic

Online-only material: animation

1. INTRODUCTION

The long-running debate on the heating of chromospheric layers by acoustic waves is fed by the fact that even the largest measured energy fluxes (found by Bello González et al. 2009, 2010) are nearly an order of magnitude smaller than the amount needed to balance the chromospheric energy losses of 14,000 W m^{-2} (Anderson & Athay 1989). Bello González et al. found an acoustic energy flux of ∼3000 W m^{-2} at 250 km and of ∼2000 W m^{-2} at 500 km from velocity fluctuations measured from narrowband (FWHM = 1.8 pm) data at ∼0.″4 spatial resolution on the Fe I lines at 557.6 nm and 543.4 nm, formed in mid-photospheric and low-chromospheric layers, respectively. This is a factor of 4–6 larger than that given by Fossum & Carlsson (2006) and Carlsson et al. (2007) from intensity fluctuations in continuum bands at 160 nm (of ∼1″ spatial resolution) and in Ca II H formed at heights of 430 km and 200 km, respectively. We refer the reader to Bello González et al. (2009) for a detailed introduction to the acoustic-wave heating debate.

In this contribution, we present results on acoustic waves from data taken on the Fe I line at 525.02 nm with the highest spatial resolution considered so far.

2. OBSERVATIONS AND DATA ANALYSIS

The data analysed in this study were taken on 2009 June 9 with the IMaX two-dimensional spetropolarimeter (Martínez Pillet et al. 2010) on board Sunrise (Barthol et al. 2010; Solanki et al. 2010). This study is performed on a time series of ∼23 minutes with 33 s cadence, taken from 00:36 UT on in full polarimetric mode, at the quiet disk center. The data consist of narrow (FWHM = 6 pm) spectropolarimetric filtergrams taken at [±8, ±4, +22.7] pm around the Fe I 525.02 nm line (Landé factor, $g = 3$). The capabilities of retrieving the physical parameters with the given spectral sampling has been studied by Orozco Suárez et al. (2010). The data were calibrated according to Martínez Pillet et al. (2010, Section 9.2) and possess a spatial resolution of 0.″15–0.″18, achieved by combining the onboard image stabilization system (Gandorfer et al. 2010; Berkefeld et al. 2010) and phase-diversity techniques (Martínez Pillet et al. 2010). The field of view (FOV) considered is 44.8 × 44.8 arcsec^2 (815 × 815 pixel^2). The line-of-sight (LOS) velocities were determined by measuring Doppler shifts of the minimum position of a Gaussian fitting the four spectral points within the Fe I line plus continuum (Martínez Pillet et al. 2010).

2.1. Response Functions

We base our study of wave phenomena on the analysis of fluctuations in the measured LOS velocities. For a better comprehension of the atmospheric layer where the Fe I line at 525.02 nm is sensitive to velocity fluctuations, we calculated velocity response functions (RF$_v$), applying the method described by Eibe et al. (2001). Following Bello González et al. (2010), we considered granule (GR) and intergranule (IGR) model atmospheres based on three-dimensional simulations from Asplund et al. (2000). Results are shown in Figure 1(a). In the case of a spectrometer with infinite spectral resolution, the RF$_v$ calculated for the line minimum in both atmospheres are centred around 400 km height, in agreement with results by Shchukina & Trujillo Bueno (2001). However, the RF$_v$ are shifted to lower layers and partly broadened when (1) the spectral transmission of the IMaX instrument and (2) the Gaussian-fit used in the determination of the line-minimum velocities, are applied to the emergent intensities in order to mimic the measurements from IMaX observations. For GR, the RF$_v$ is centred at ∼325 km and for IGR at ∼175 km.

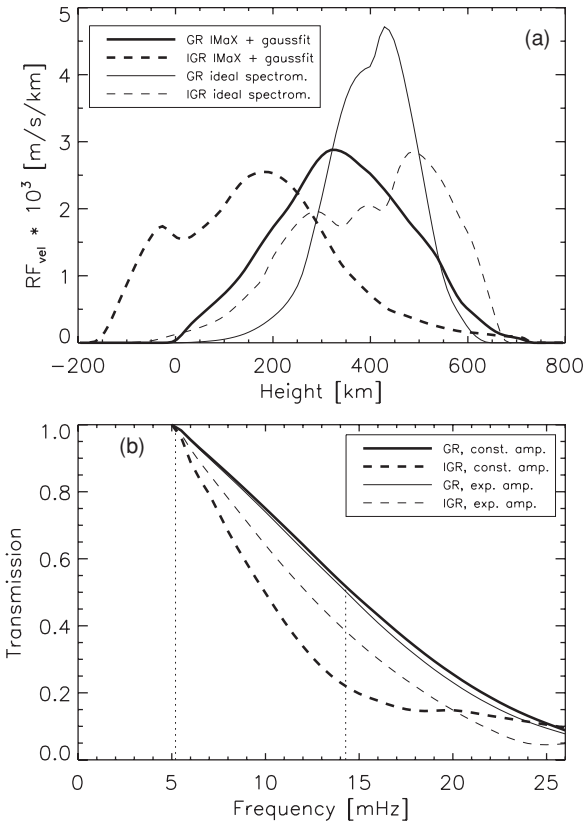

Figure 1. (a) Response functions for velocity $\mathrm{RF}_\upsilon(z)$ at line minimum of Fe I 525.02 nm: solid and dashed, for granule (GR) and intergranule (IGR) atmospheres, respectively; thick, after convolution of line profiles with spectrometer function and Gaussian fit, to mimic the IMaX observed profiles. (b) Transmission of solar atmosphere to wave (velocity) amplitudes vs. wave frequency after convolution with the spectral transmission of the IMaX instrument; solid: GR, dashed IGR; thick: waves/ with amplitudes constant in height; thin: waves with exponentially increasing amplitude. Dotted lines indicate the frequency (acoustic) range under study, i.e., from the acoustic cut-off frequency, $\nu_{ac} = 5.2$ mHz ($U = 192$ s) up to $\nu = 14.3$ mHz ($U = 70$ s).

2.2. Atmospheric Transmission to Velocity Amplitudes

The broad extent in height of the RF_υ indicates the large atmospheric range where the measured velocities are referred to, i.e., indicates the difficulties in detecting the signal of small-scale velocity fluctuations along the LOS. It is then advantageous to estimate the transmission of the solar atmosphere to (wave) velocity amplitudes, i.e., the ratio of the observed to actual velocities, taking into account the spectral characteristics of our optical system and the velocity determination method.

The transmission function is modeled by computing velocities from synthesised IMaX profiles from a model atmosphere including velocity fluctuations (waves) along the LOS. We consider both the GR and IGR atmospheres following two approaches: (1) waves with height-independent amplitude and (2) with exponentially increasing velocity amplitudes. The latter mimics an acoustic energy flux constant through the stratified atmosphere. We refer to Bello González et al. (2009, 2010) for detailed descriptions on the transmission function calculations and the determination of group velocities derived from the dispersion relation of waves.

Figure 1(b) depicts the resulting functions. They show similar transmissions for the GR atmosphere when considering height-independent or exponentially increasing velocity amplitude. The IGR atmosphere shows a lower transmission for waves with height-independent amplitude. Lower transmission means larger correction in the determination of the energy flux (see Section 3.1).

3. RESULTS

We performed Fourier and wavelet analyses of the velocity fluctuations over the time series, as in Bello González et al. (2009, 2010). The temporal power spectra were calculated at each pixel and averaged over the FOV. A separate study on GR and IGR areas has been performed. GRs are considered to be those regions in the continuum intensity maps where $I_{\mathrm{cont}}/\langle I_{\mathrm{cont}}\rangle > 1$ and IGRs where $I_{\mathrm{cont}}/\langle I_{\mathrm{cont}}\rangle < 1$. GR dark dots and forming lanes are thus treated as IGRs.

3.1. Acoustic Energy Flux

The total flux of acoustic energy (per element of area on the Sun) is estimated from the spatially averaged Fourier power $P_\upsilon(\nu_i)$ by

$$F_{\mathrm{ac,tot}}(\nu_i) = \rho \sum_i P_\upsilon(\nu_i) \cdot \upsilon_{\mathrm{group}}(\nu_i)/T(\nu_i) \cdot \Delta\nu_i \,, \qquad (1)$$

with mass density ρ, group velocity $\upsilon_{\mathrm{group}}$, and frequency intervals $\Delta\nu_i$. $T(\nu)$ represent the transfer functions, i.e., the square of the transmission functions in Figure 1(b). Note that the transfer functions express the smoothing by radiative transfer for small wavelengths and we correct our measurements from this effect. From the GR and IGR models, we adopt the values $\rho_{\mathrm{GR}} = 5.9 \times 10^{-5}$ kg m^{-3} at 325 km and $\rho_{\mathrm{IGR}} = 10^{-4}$ kg m^{-3} at 175 km. We limit our study to the acoustic frequency range, i.e., from 5.2 to 15.1 mHz, the latter value being the Nyquist frequency of our observations.

Wavelets are an appropriate tool to retrieve information on the distribution of power in space and time. With this technique, we calculated two-dimensional maps of power spectra in period bins of 20 s from 70 s up to 190 s, i.e., the acoustic cutoff period. We employed the code by Torrence & Compo (1998) with Morlet wavelets and a level of significance of 95%. An analogous equation to Equation (1) is then used in terms of periods U (with $\Delta U_i = 20$ s) to determine the acoustic flux from the wavelet power averaged over time and FOV.

Figure 2 shows averages of velocity flux spectra as functions of period (frequency) from the wavelet and Fourier analyses. We differentiate between GR (thin) and IGR (thick) fluxes before (dashed) and after (solid) the correction of atmospheric transmission, in the case of exponentially increasing amplitudes. This correction is more conservative than that for waves with height-independent amplitude (see Figure 1(b)), therefore it will provide us with lower limit corrected estimates. For the differentiation, we obtain the power above GRs and IGRs from the wavelet analysis (cf. Figure 3). The resulting weights are transferred to the power in the Fourier analysis (see Bello González et al. 2010).

Before correction, we find in both the Fourier and wavelet analyses, an IGR flux larger than the GR flux by a factor 1.7. The correction increases the flux in the IGR more strongly, as expected from the transmission functions (Figure 1(b)). After the correction, the ratio between IGR and GR fluxes amounts to 1.8–2.0.

The results on the total acoustic flux summed over all frequencies are collected in Table 1. The "average" values refer to the flux over the FOV filled by GR over 46% of the area

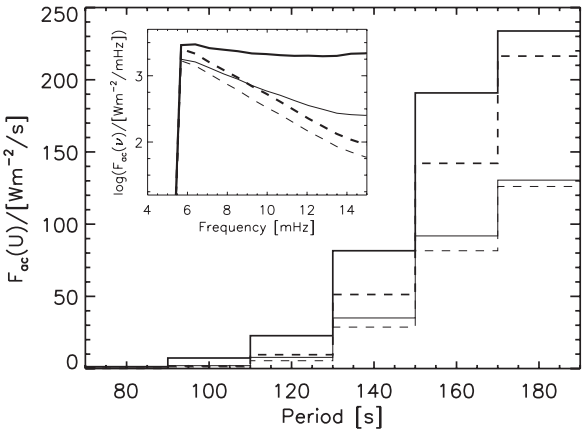

Figure 2. Velocity flux spectra from wavelet (vs. period) and Fourier (vs. frequency) analysis. Thin and thick represent GR and IGR spectra, before (dashed) and after (solid) correction for atmospheric transmission, respectively.

Table 1
Total Acoustic Energy Fluxes, $F_{ac,tot}$ (W m^{-2})

Wavelet	Uncorr.	Corrected
GR	4430	5000–4970
IGR	6400	7725–8630
Average	5495	6470–6945
5.2–10 mHz	5455	6360–6765
10–14.3 mHz	40	110–180
Fourier	Uncorr	Corrected
GR	4930	7000–6865
IGR	7540	13075–20165
Average	6340	10280–14050
5.2–10 mHz	5630	7720–8900
10–14.3 mHz	710	2560–5150

Note. Left and right values in column corrected refer to the exponentially increasing and height-independent velocity amplitude approaches, respectively (Section 2.2).

and by IGR over the remaining 54%. Results from the wavelet and Fourier analyses agree for the most part at low frequencies, i.e., for periods $\geqslant$100 s. They amount to $\sim$5500 W m^{-2} before correction and to $\sim$6400–7700 W m^{-2} after the conservative correction. Yet, a large difference appears at high frequencies, where the treatment of the Fourier and wavelet analysis is different: (1) the wavelet approach is more restrictive in terms of noise when using a statistical significance level of 95%, therefore the retrieved values at these frequencies are low, (2) the wavelets were applied in period bins which reduces the spectral sampled points at high frequencies to just the bin at 80 s and half of the bin at 100 s, and (3) the values at high frequencies are strongly corrected, i.e., the originally larger values in the Fourier analysis spectra are highly increased.

We are confident in the correction of the flux spectra for frequencies $\leqslant$10 mHz. The large correction of flux for frequencies $>$10 mHz above IGRs from the Fourier analysis, see the inset in Figure 2, turns the flux spectrum upward. This also was noted by Fleck et al. (2008) who point out the difficulty in determining the noise level. In addition, aliasing from power at frequencies above our Nyquist frequency may play a role. With these caveats, we consider the large fluxes at high frequencies as upper limits. The high-frequency waves are most prone to radiative damping. Their amplitudes will thus be strongly reduced at the base of the chromosphere.

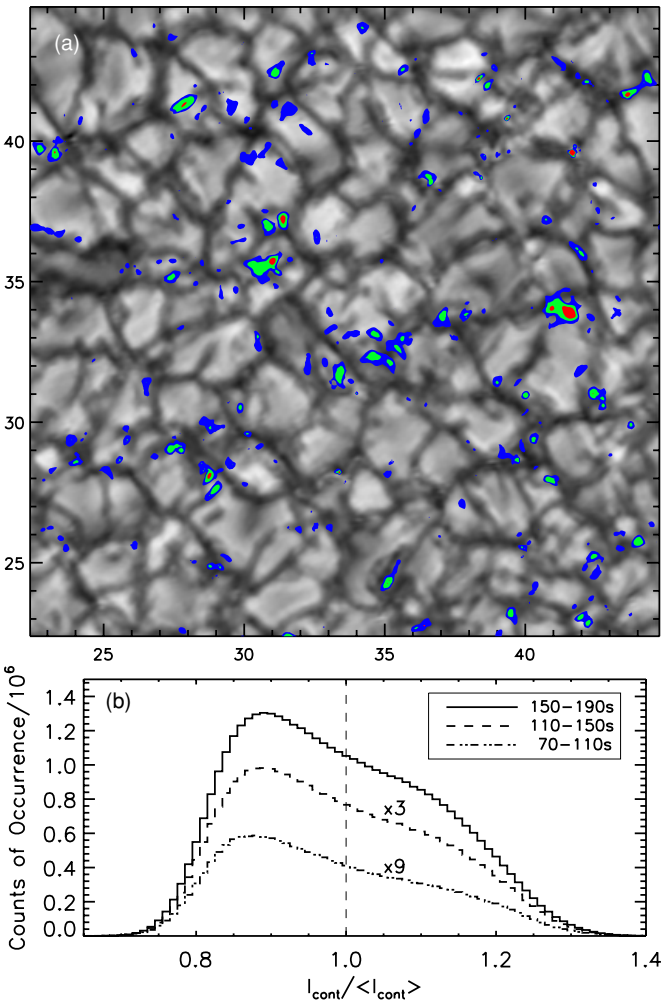

Figure 3. (a) Snapshot on acoustic power averaged over the period range [150–190] s, overlaid on a continuum image. The area corresponds to the upper-right quadrant of the full FOV; filled contours represent 12% (blue), 20% (green), and 32% (red) of the maximum power value over the sequence; tickmarks in arcsec. The underlying animation is available in the online edition of the journal. (b) Occurrence of wavelet power of velocities above 1% of maximum power vs. normalized continuum intensities $I_{cont}/\langle I_{cont}\rangle$ for reconstructed data. Curves for [110–150] s and [70–110] s period bins were amplified by factors of three and nine, respectively, for better visualisation.
(An animation of this figure is available in the online journal.)

In any case, even before correction, the directly measured energy fluxes are larger than those found in any previous observational study of acoustic waves. The nature of these results and their consequences are discussed in Section 4.

3.2. Spatial Distribution of the Acoustic Flux

The wavelet analysis provides maps of wave power for each time step. With this technique applied to the high-spatial resolution IMaX data, we can study in detail the distribution of power (flux) over the observed FOV and its evolution with time. Figure 3 shows an example of different levels of acoustic power over the period range [150–190] s overlaid on continuum images, and an animation of the time evolution of such power patches is available in the online edition of the journal.

The time lag corresponding approximately to the travel time from the bottom of the photosphere to 250 km height is about 42 s. The cadence of the time series is 33 s, therefore no delay between intensity and power maps has been taken into account.

The wave power, far from being homogenously distributed, appears intermittently in space and time as already found by, e.g., Rimmele et al. (1995), Wunnenberg et al. (2002), and Bello González et al. (2009, 2010). Histograms of the acoustic power occurrence over intensity represented in Figure 3 show that most of the power, at all frequencies, is associated with dark structures, i.e., structures with intensities $I_{\rm cont}/\langle I_{\rm cont}\rangle < 1$. We have referred to these structures as IGRs, but close inspection of the power maps overlaid on the continuum intensities (see the animation associated with Figure 3) reveal that significant power is found in forming GR (dark) dots and lanes. A second, less prominent component or shoulder is seen in the histograms at $I_{\rm cont}/\langle I_{\rm cont}\rangle \sim 1.1$. It has not been reported before, we see it thanks to the high contrast of the IMaX images. This power is found in small rapidly evolving GRs and in large GRs: (1) prior to their splitting and (2) at their bright borders. Yet not all splitting GRs and bright borders show a wave power component.

3.3. Energetic Fast-fluctuating Features

Studying the evolution of acoustic power reveals patches of intense signal. They appear intermittently and randomly distributed, covering areas of typically 1 arcsec^2 and with power at all periods lasting for about 5 minutes. Such strong signals are found to be generated by rapid fluctuations in velocities up to $\sim$4 km s^{-1}, which are of a diverse nature: (1) sudden (within 2–3 minutes) up-down-up flows, (2) sudden down-up-down flows, (3) some associated to magnetic field concentrations, (4) some with no significant magnetism, and (5) some of the latter related to imploding GR areas, etc.

In a first analysis, we have identified 32 of these events within the 23 minute series. Masking these events and calculating the acoustic flux from their wave power, we find that they carry 20–23 kW m^{-2} (estimated values before and after correction, respectively). Yet, their small area coverage, 0.1% of the FOV, implies that their global contribution to the total flux is not significant.

Nevertheless, the identification of these energetic features at small scales from their strong power signature has opened a new field of study and we refer to a forthcoming contribution on the nature of these events.

4. DISCUSSION AND CONCLUSIONS

In this study, we have taken advantage of the high quality data of the IMaX/Sunrise instrument. The high spatial resolution provided new exciting findings, which (1) confirm that acoustic waves play an important role in the energy transport through the quiet solar atmosphere, (2) shed new light on the spatial and temporal distribution of propagating wave phenomena, and (3) reveal the existence of very energetic processes occurring at small scales.

Table 2 summarizes the values of acoustic energy flux measured by different authors in the last years. Averaged values from the present study before and after correction of the transmission of the solar atmosphere to the velocity wave amplitudes are also listed for comparison.

We note that the use of transmission functions for correcting velocity amplitudes at short periods is controversial. The results from three-dimensional hydrodynamic simulations by Fleck et al. (2010) suggest that the observed high-frequency Doppler shifts are caused by rapid variations of the contribution functions in an atmosphere with high velocity gradients. These authors conclude that one should re-evaluate the cause of Doppler shifts with periods $\leqslant$70 s, i.e., periods below the Nyquist period of our observations.

Table 2
Summary of Observed Total Acoustic Flux $F_{\rm ac,tot}$ (Wm^{-2}).

Method/Data	Uncorr.	Corrected
Wavelet: binned (2 × 2)	3975	4600–4900
Wavelet: binned (1 × 1)	5495	6470–6945
Fourier: binned (1 × 1)	6340	10280–14050
Other work		
Bello González et al. (2010)		
h = 500–600 km, 0.″4	···	1700–2000
Bello González et al. (2009)		
h = 250 km, 0.″4	2500	3000–3650
Straus et al. (2008)		
h = 250 km, ∼ 0.″4	···	1400
h = 500 km, ∼ 0.″5	···	1000
Carlsson et al. (2007)		
h = 200 km, ∼ 0.″22	···	800
Fossum & Carlsson (2006)		
h = 430 km, ∼ 1″	···	510
Wunnenberg et al. (2002)		
h = 600 km, ∼ 0.″5	···	900

Note. Notation in column *corrected* as in Table 1.

We restrict the following discussion to the flux values from the wavelet analysis, which we consider to be lower limits. The average acoustic flux at 250 km is $F_{\rm ac,tot} \sim 6500$ W m^{-2}, after a conservative[8] correction. It is mainly found at low frequencies (periods $\geqslant$100 s). Yet, the uncorrected flux already amounts to 5500 W m^{-2}. These large values were never reported before, probably due to limited spatial resolution. Wedemeyer-Böhm et al. (2007) pointed out from three-dimensional simulations that a significant amount of acoustic power is lost when degrading the spatial resolution. This effect can be seen when applying to our data a 2 × 2 pixel binning. The signal is reduced by a factor of 1.4. We note that Carlsson et al. (2007), analysing *HINODE* data, found a lower power reduction upon binning. Also compare the resulting acoustic flux with that found by Bello González et al. (2009) at the same height. There the spatial resolution is at least a factor of two less, although the spectral sampling is better. After transmission correction, the IMaX data provide fluxes larger by a factor of two. We conclude that much of the power in the quiet Sun occurs at small scales and high spatial resolution is mandatory to detect it.

Simulations by Straus et al. (2008) give an estimate of 30% for energy losses between 250 km up to 500 km due to radiative damping. Applying the same correction, the averaged acoustic flux we observe at 250 km would then be reduced to 4500 W m^{-2} at the bottom of the chromosphere. On the one hand, the flux reduction between 250 km and 500 km may be larger because of the very small spatial scales in the present data set. On the other hand, the estimated flux at 250 km is only a lower limit value since we have considered: (1) wavelet power and (2) the conservative correction. This acoustic flux is comparable to the radiative losses of 4600 W m^{-2} quantified from the standard semi-empirical hydrostatic model of a quiet average chromosphere by Vernazza et al. (1981). Chromospheric models calculated including radiative losses from Fe II lines, arrive at energy needs of 14000 W m^{-2} (Anderson & Athay 1989).

[8] Conservative stands for the less restrictive correction when calculating transfer functions for exponentially increasing velocity amplitudes, Section 2.1.

In our wavelet analysis, the contribution from high-frequency (>10 mHz) waves is missing, but likely present in the solar atmosphere as suggested, e.g., the Fourier analysis.

Let us recall the main findings of this first study on acoustic waves from IMaX/SUNRISE observations at the diskcenter.

1. The improvement of at least a factor of two in spatial resolution and the image quality of IMaX/SUNRISE data have revealed a total acoustic power larger by at least a factor of two than the largest power observed before. In view of the results obtained on the total acoustic power, we conclude that, at photospheric level, acoustic waves with periods >100 s carry at least half of the flux needed to balance the observed radiative energy losses of the quiet chromosphere according to Anderson & Athay (1989). The possibility that the quiet solar chromosphere is supplied with acoustic wave energy to cover its radiative losses, as suggested many years ago by L. Biermann and M. Schwarzschild and later on pursued intensively by P. Ulmschneider, needs to be revived and intensively studied, probing which fraction of the transported energy reaches the chromosphere.
2. The main contribution to the acoustic energy flux is found in IGRs, as is extensively known. In addition, forming dark dots and lanes above splitting GRs as well as small fast-evolving GRs and the brighter borders of large GRs are found to be sources of propagating waves. These are regions of strong dynamics (turbulence) as pointed out in the studies on the same IMaX data series by Steiner et al. (2010), and Roth et al. (2010).
3. Thanks to the high quality of the IMaX data, it has been possible to detect intermittent sources of strong energy fluxes at all frequencies in the acoustic domain. A preliminary analysis of their nature shows that they are generated by rapid (2–3 minute) fluctuations in their LOS velocity occurring at small scales, i.e., typically of $0\farcs3 \times 0\farcs3$. They show a diverse origin, in some cases they are related to small magnetic field concentrations, in others to imploding GRs, etc. We refer to a forthcoming contribution for a detailed analysis of these events.

N.B.G. thanks F. Kneer for his invaluable help and interest in this work. N.B.G. also thanks R. Schlichenmaier and B. Louvel for helpful suggestions on the manuscript. The German contribution to SUNRISE is funded by the Bundesministerium für Wirtschaft und Technologie through Deutsches Zentrum für Luft- und Raumfahrt e.V. (DLR), Grant No. 50 OU 0401, and by the Innovationsfond of the President of the Max Planck Society (MPG). The Spanish contribution was funded by the Spanish MICINN under projects ESP2006-13030-C06 and AYA2009-14105-C06 (including European FEDER funds). The HAO contribution was partly funded through NASA grant number NNX08AH38G. Support by the WCU grant no. R31-10016 by the Korean Ministry of Education, Science and Technology is acknowledged. The National Center for Atmospheric Research is sponsored by the National Science Foundation.

REFERENCES

Anderson, L. S., & Athay, R. G. 1989, ApJ, 346, 1010
Asplund, M., Nordlund, Å., Trampedach, R., & Stein, R. F. 2000, A&A, 359, 743
Barthol, P., et al. 2010, Sol. Phys., in press (arXiv:1009.2689)
Bello González, N., Flores Soriano, M., Kneer, F., & Okunev, O. 2009, A&A, 508, 941
Bello González, N., Flores Soriano, M., Kneer, F., Okunev, O., & Shchukina, N. 2010, A&A, in press
Berkefeld, T., et al. 2010, Sol. Phys., in press (arXiv:1009.3196)
Carlsson, M., et al. 2007, PASJ, 59, 663
Eibe, M. T., Mein, P., Roudier, T., & Faurobert, M. 2001, A&A, 371, 1128
Fleck, B., Jefferies, S. M., McIntosh, S. W., Severino, G., Straus, T., & Tarbell, T. D. 2008, in 12th ESP Meeting, Freiburg, Germany, http://espm.kis.uni-freiburg.de
Fleck, B., Straus, T., Carlsson, M., Jefferies, S. M., Severino, G., & Tarbell, T. D. 2010, in Proc. 25th NSO Workshop, ed. A. Tritschler, K. Reardon, & H. Uitenbroek, Mem. Soc. Astron. Ital., in press
Fossum, A., & Carlsson, M. 2006, ApJ, 646, 579
Gandorfer, A., et al. 2010, Sol. Phys., in press (arXiv:1009.1037)
Martínez Pillet, V., et al. 2010, Sol. Phys., in press (arXiv:1009.1095)
Orozco Suárez, D., Bellot Rubio, L. R., Martínez Pillet, V., Bonet, J. A., Vargas Domínguez, S., & del Toro Iniesta, J. C. 2010, arXiv:1006.5510
Rimmele, T. R., Goode, P. R., Harold, E., & Stebbins, R. T. 1995, ApJ, 444, L119
Roth, M., et al. 2010, ApJ, 723, L175
Shchukina, N., & Trujillo Bueno, J. 2001, ApJ, 550, 970
Solanki, S. K., et al. 2010, ApJ, 723, L127
Steiner, O., et al. 2010, ApJ, 723, L180
Straus, T., Fleck, B., Jefferies, S. M., Cauzzi, G., McIntosh, S. W., Reardon, K., Severino, G., & Steffen, M. 2008, ApJ, 681, L125
Torrence, C., & Compo, G. 1998, Bull. Am. Meteor. Soc., 61, 79
Vernazza, J. E., Avrett, E. H., & Loeser, R. 1981, ApJS, 45, 635
Wedemeyer-Böhm, S., Steiner, O., Bruls, J., & Rammacher, W. 2007, in ASP Conf. Ser. 368, The Physics of Chromospheric Plasmas, ed. P. Heinzel, I. Dorotovič, & R. J. Rutten (San Francisco, CA: ASP), 93
Wunnenberg, M., Kneer, F., & Hirzberger, J. 2002, A&A, 395, L51